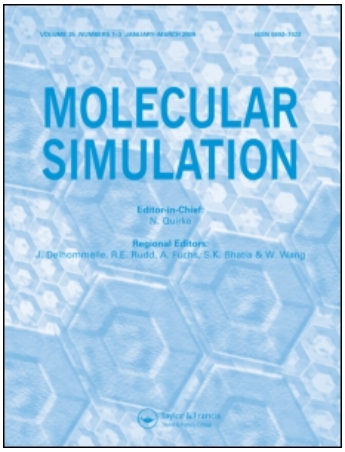

Molecular Simulation
Publication details, including instructions for authors and subscription information:
http://www.informaworld.com/smpp/title~content=t713644482

Orientation effects of elastic-plastic deformation at surfaces: nanoindentation of nickel single crystals

Oyeon Kum

To cite this Article Kum, Oyeon(2005) 'Orientation effects of elastic-plastic deformation at surfaces: nanoindentation of nickel single crystals', Molecular Simulation, 31: 2, 115 — 121
To link to this Article: DOI: 10.1080/08927020412331308502
URL: http://dx.doi.org/10.1080/08927020412331308502

Molecular Simulation, Vol. 31, No. 2–3, 15 February–15 March 2005, 115–121

Taylor & Francis
Taylor & Francis Group

Orientation effects of elastic–plastic deformation at surfaces: nanoindentation of nickel single crystals

OYEON KUM*

Department of Chemistry, Clemson University, Clemson, SC 29634, USA

(Received March 2004; in final form July 2004)

Molecular dynamics simulations were performed to study anisotropic features in nanomechanical properties at the surfaces of nickel single crystals as a function of indenter size and velocity for three crystallographic orientations: ⟨100⟩, ⟨110⟩, and ⟨111⟩. The tabular form of Voter's embedded atom method (EAM) potential was used to describe the interatomic interactions of nickel single crystals. A strongly repulsive potential model between the indenter tip and the metal surface was designed to address the effect of a passivation layer. The force vs. displacement curves for indentation followed the power law solution of $F = k\delta^{\nu}$ for elastic deformation. The value of ν was dependent on the indenter velocity, following the Hertzian solution ($\nu = 1.5$) at the high velocity of approximately 670 m/s but showing a non-Hertzian power ($\nu = 2.5$) at the low velocity of approximately 67 m/s. The force fitted micro-modulus showed a dependency on indenter size and velocity for the three crystallographic orientations. The results of dislocation nucleation—the early stage of plasticity—in the different orientations showed anisotropy: stacking faults in the ⟨100⟩ orientation, deep partial dislocations in the ⟨110⟩ orientation, and shallow partial dislocations followed by stacking faults in the ⟨111⟩ orientation.

Keywords: Nanoindentation; Anisotropy; Indentation curve; Dislocation nucleation; Elastic–plastic deformation; Nickel single crystal

1. Introduction

Considerable attention has been devoted recently to understanding of the connection between atomic scale processes and the measurable mechanical properties of materials. One of the most interesting computational challenges for the atomistic calculations of material properties is to investigate the mechanical deformation, fracture, and friction of solids and thin films. My recent studies of large-scale simulations of single nickel crystals using Morse-type pair potentials, the analytical form of embedded atom method (EAM) potential, and the tabular form of the EAM potential under shock compressed conditions [1,2] represent a good start toward a more realistic study of materials using atomistic methods. Specifically, understanding the mechanical behavior under the surface of small volume nickel crystals as they come into contact with an indenter is becoming increasingly important from both scientific and technological viewpoints. Nickel is one of the favored materials for either reactively or catalytically forming a smooth electroless deposition of additional thin layers to provide enhanced magnetic read–write capability on magnetic memory disks [3].

In nanoindentation experiments, an interfacial force microscope and atomic-force microscopy are used to investigate the detailed mechanisms of deformation during indentation at a very small scale. Such experiments are usually used not only to measure the nano-mechanical properties, for example, the hardness or the Young's modulus, but also to study the dislocation nucleation at the nanometer level, although the stress and strain distribution associated with indentations is still poorly understood, especially in crystalline solids exhibiting well-defined slip systems such as fcc single crystals. Modern nanoindentation techniques have allowed for the measurement of load or force on the indenter tip as a function of tip displacement during indentation and retraction where the contact radius is less than 100 nm [4]. These small volumes are appropriate for large-scale molecular dynamics simulations for making direct comparisons between experiments and simulations. Such comparisons may solve the discrepancies among different models and experiments. For example, a typical nanoindentation curve exhibits abrupt bursts in displacement at a constant load in the region of the positive slope, whereas, a classical curve shows a relatively smooth positive slope.

Molecular Simulation
ISSN 0892-7022 print/ISSN 1029-0435 online © 2005 Taylor & Francis Group Ltd
http://www.tandf.co.uk/journals
DOI: 10.1080/08927020412331308502

Such discrepancies are postulated to result from the discrete nucleation of dislocation loops below the indenter, but the exact mechanisms, which are still under discussion, are difficult to investigate experimentally [5].

Previous atomistic simulations using EAM potentials or other semiempirical potential models, as well as first-principle methods [6–8], showed strong bonding between the indenter tip and the surface due to the large energy of adhesion between two clean surfaces. This phenomena leads to a jump to contact when the indenter approaches and a necking between the tip and surface during retraction appears [9]. However, this tip–surface adhesion interaction in experiments is dramatically reduced because either is not atomically cleaned or the surfaces are passivated by the addition of an alkanethiol layer that prevents bonding between the two. To address this issue, this paper presents a computational model describing a frictionless indenter represented by a strong repulsive potential for atomistic calculations to study elastic and plastic deformation during indentation on a passivated surface. This series of simulations provides a new insight into the initial stages of plastic deformation.

Almost all metals are somewhat elastically anisotropic, a property that makes nanoindentation measurements complicated. The purpose of this work was both to gain insight into the yielding phenomena in atomistic scale processes and to examine the anisotropy at the early stages of plasticity involved in the deformation of nickel single crystals for three crystallographic orientations: ⟨100⟩, ⟨110⟩ and ⟨111⟩. Using the large-scale molecular dynamics code (double-SPMD code [2]), the typical micromechanical parameter of micro-modulus and its dependency on indenter size, velocity, and crystallographic orientations were calculated. In addition, the anisotropic features of dislocation nucleation—the early stage of plasticity—in the different orientations were studied. The organization of this paper is as follows. In Section 2, the atomic interaction of the EAM potential and the indenter tip–surface interaction model are described in detail. In Section 3, the loading curves using power law solutions and deformation phenomena in three crystallographic orientations are analyzed. Finally, Section 4 is devoted to the conclusions of this study.

2. The model

Since a typical dislocation separation is the order of μm for well-annealed metals, the area under the nanoindenter should behave close to that of a perfect single crystal, i.e. dislocation free. Voter's tabular form of the EAM potential model was employed to describe the atomic interactions of nickel single crystals. Since this potential model is described in detail elsewhere [10], only a brief summary is provided here. In metals, not all electrons are localized at the nuclei, with the valence electrons often being shared among many ions, suggesting a nearly free-electron gas. The EAM potential describes the embedding energy as a function of the background electron density and the atomic species. The total energy (E_{tot}) of a system of N atoms is written as a sum of the atom energies:

$$E_{\text{tot}} = \sum_{i}^{N} E_i. \tag{1}$$

In the embedded atom method, E_i is given by

$$E_i = \frac{1}{2}\sum_{j} \phi_{ij} + F(\overline{\rho}_i), \tag{2}$$

with

$$\overline{\rho}_i = \sum_{j} \rho(r_{ij}), \tag{3}$$

where r_{ij} is the distance between atom i and atom j, ϕ is the pairwise interaction between atoms. ρ is the pairwise interaction leading to the density term $\overline{\rho}_i$ of the embedding function, $F(\overline{\rho})$. The key to EAM is the nonlinearity of the function $F(\overline{\rho})$, which, thus, provides the many-body contribution to the energy attributed to the shared nearly free-electron gas.

Voter's nickel EAM potential, employed here, reproduces the bulk lattice constant, cohesive energy, elastic constants, and vacancy formation energy, as well as the bond formation energy and bond length of the gas phase nickel dimer, as shown in table 1. Though the potential model has been proven to be successful in solving many problems, including the melting behavior, the structure of small nickel clusters on nickel surfaces, the thermodynamic properties of liquid nickel, the large-scale fracture dynamics studying the dislocation emission from a three-dimensional crack, and the surface-diffusion, [11–14] there has been little if any study of the energetics of stacking faults and yield stresses caused by the dislocation nucleation. Therefore, it is significant that this investigation provides new insights into the atomistic processes resulting from the deformation of nickel single crystals.

Previous atomistic calculations have studied indentation and retraction using EAM potentials [6], other semiempirical potential models [7], or first-principle methods [8]. These calculations have shown a strong

Table 1. Experimental input and best-fit calculated properties for the EAM nickel potential [10]

Property	Calculated	Experimental
a_0 (Å)	3.52	–
E_{coh} (eV)	4.45	–
B (10^{12} erg/cm^3)	1.80	–
C_{11} (10^{12} erg/cm^3)	2.44	2.47
C_{12} (10^{12} erg/cm^3)	1.48	1.47
C_{44} (10^{12} erg/cm^3)	1.26	1.25
$\Delta E^{\text{f}}_{\text{ly}}$ (eV)	1.6	1.6
R_e (Å)	2.23	2.2
D_e (eV)	1.94	1.95

The fitting procedure reproduces a_0, E_{coh}, and B exactly. The root-mean-square fitting error for the remaining data is about 1.2%.

bonding between the indenter tip and the surface because of the large amount of adhesion energy between two clean surfaces, causing a jump to contact when the indenter approaches and a necking between the tip and surface during retraction. However, the tip–surface adhesion interaction was found to be reduced dramatically in experiments because each was not atomically clean or their surfaces were passivated by the addition of an alkanethiol layer which prevents the bonding [15]. In this study, a strongly repulsive potential model between the indenter tip and the metal surface was designed to simulate the passivated surface. Each atom in the indented material interacted with the idealized spherical indenter via the following repulsive potential:

$$V(r) = \epsilon(\sigma/r)^{\alpha}, \tag{4}$$

where ϵ is energy, σ is the indenter radius, r is the distance between an atom and the center of the indenter, and α is the power of the potential. In the simulations, α was 150 to guarantee a strongly repulsive force between the indenter and the surface. As is customary, reduced (or dimensionless) quantities were used to specify various physical parameters. The energy unit is eV, the unit of length is Å, and the unit of mass is the atomic unit of nickel. Thus, the time unit $t_0 = (m\sigma^2/\epsilon)^{1/2}$ and the force unit is 43.59042 (nN).

3. Results and discussion

Simulations were performed for two indenter diameters (5.0 and 6.0 nm) and two indenter velocities (approximately 670 and 67 m/s). The indenter approached the cold (zero temperature) fcc nickel single crystals oriented in the ⟨100⟩, ⟨110⟩ and ⟨111⟩ directions. The total number of atoms involved were 400,000, 397,600 and 397,440 for the ⟨100⟩, ⟨110⟩, and ⟨111⟩ orientations, respectively. Figure 1 shows the indented nickel single crystals for these three orientations. As the figure shows, the orientation-dependent pattern of the surface deformation is the diamond shape for the ⟨100⟩ indentation, the circular shape with star fish shape boundary for the ⟨110⟩ indentation, and the triangular shape for the ⟨111⟩ indentation.

Figure 2 shows the indentation force (F) vs. the displacement depth (δ) curves for the three crystal orientations for the indenter diameter of 5.0 nm and its velocity of approximately 670 m/s. In the top panel, the typical features of the curves for the three orientations are elastic deformations followed by plastic deformations. All three curves have displacement excursions that correspond to the initiation of the plastic deformation (yield points). Overall, the indentation curves follow the Hertzian solution for elastic deformation which is the power law of $F = k\delta^{\nu}$, where $\nu = 1.5$. The values of k, corresponding to the indentation modulus or micro-hardness, are 0.40, 0.52 and 0.53 for the ⟨100⟩, ⟨110⟩, and ⟨111⟩ orientations, respectively. The bottom panel shows the Hertzian curve fit to the elastic deformation in the ⟨110⟩ orientation.

The force vs. displacement curves of the three crystal orientations for the indenter diameter of 6.0 nm and its velocity of approximately 670 m/s are shown in the top panel in figure 3. As can be seen, the larger indenter produces higher micro-hardness. The values of k are 0.49, 0.64 and 0.66 for the ⟨100⟩, ⟨110⟩ and ⟨111⟩ orientations,

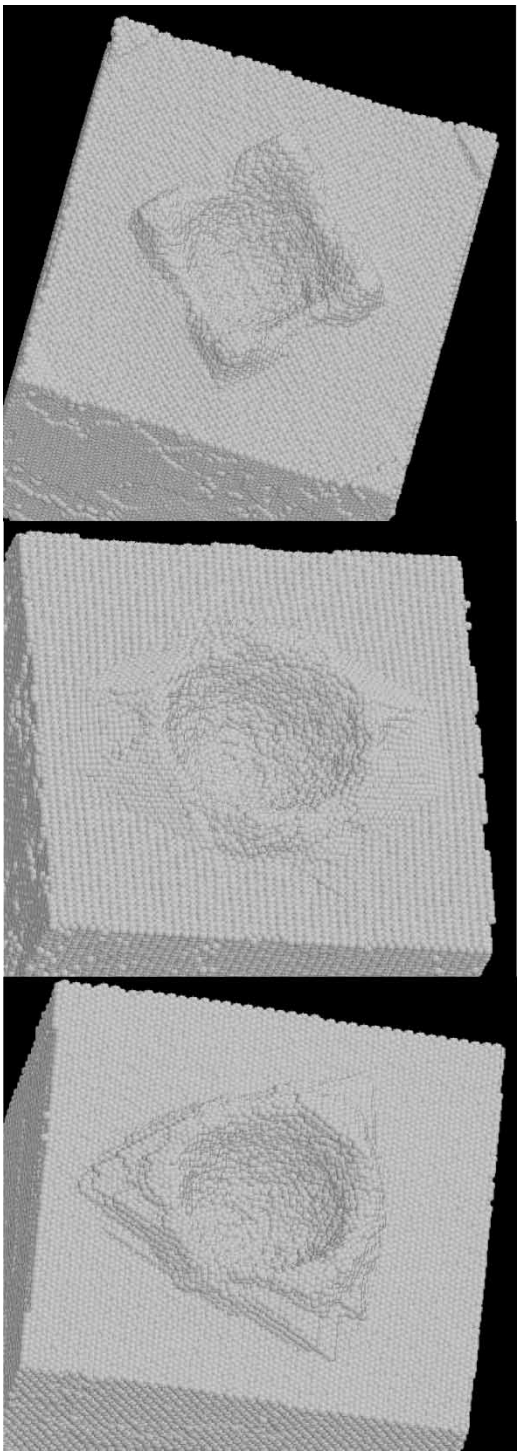

Figure 1. The indented nickel single crystals from top to bottom are the ⟨100⟩, ⟨110⟩, and ⟨111⟩ orientations, respectively. The indenter velocity is approximately 670 m/s and its diameter is 6.0 nm.

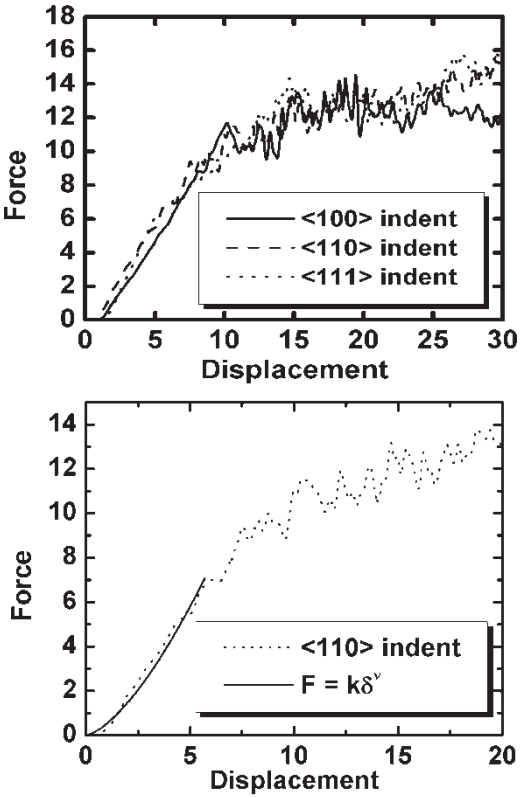

Figure 2. Top panel: indentation force vs. displacement curves in the three orientations. The indenter velocity is approximately 670 m/s and its diameter is 5.0 nm. Bottom panel: hertzian power law curve fit to the elastic deformation in the ⟨110⟩ indentation, where $k = 0.40$ and $\nu = 1.5$. The force unit is 43.59042 nN and the length unit is Å.

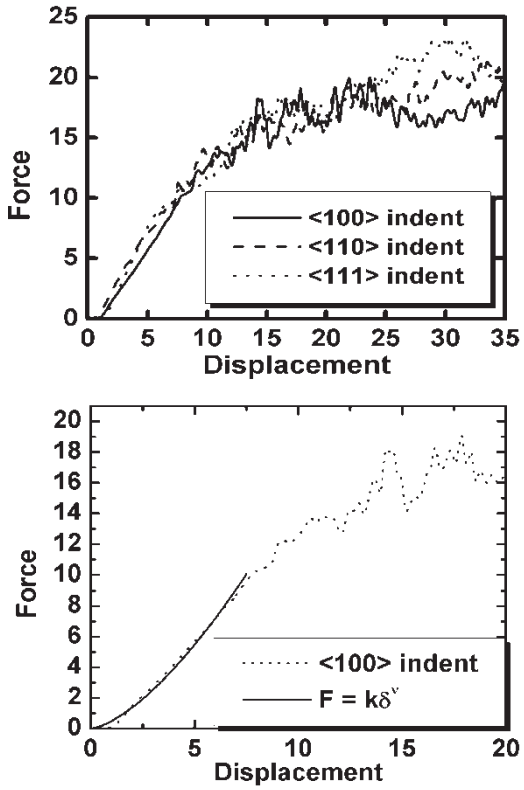

Figure 3. Top panel: indentation force vs. displacement curves in the three orientation directions. The indenter velocity is approximately 670 m/s and its diameter is 6.0 nm. Bottom panel: hertzian power law curve fit to the elastic deformation in the ⟨100⟩ indentation, where $k = 0.45$ and $\nu = 1.5$. See figure 2 caption for units.

respectively. The anisotropy is shown clearly in the different orientation directions. Comparing with figure 2, it can be seen that indenter size is considered an important parameter of anisotropy. The bottom panel shows the Hertzian curve fit to the elastic deformation in the ⟨100⟩ orientation. In figures 2 and 3, Hertzian power law solutions explain the elastic deformation for both indenter sizes.

Figure 4 shows the indentation force vs. the displacement curves for the three orientations at the indenter velocity of approximately 67 m/s and a diameter of 5.0 nm. Compared with the results shown in figure 2, a slower velocity indenter resulted in slowly varying microscopic modes of indentation curves in the region of elastic deformation initiation. The top panel shows the different excursion points for each direction: the yield strength of the ⟨110⟩ orientation was the weakest, while that of the ⟨100⟩ orientation was the strongest with the ⟨111⟩ orientation being the average. The results suggest three modes of dislocation nucleation, requiring high energy for stacking faults and relatively low energy for partial dislocations. The force is better fitted with the higher power solution, $F = k\delta^{\nu}$, where $\nu = 2.5$. Therefore, the Hertzian solution for describing the elastic deformation is no longer valid. The values of k are 0.05, 0.09 and 0.06 in the ⟨100⟩, ⟨110⟩, and ⟨111⟩ orientations, respectively. The bottom panel shows the higher power law solution ($\nu = 2.5$) in the range of elastic deformation initiation in the ⟨111⟩ orientation. Thus, the force vs. displacement curves show a strong dependency on indenter velocity.

The centrosymmetry parameter, defined below, [9] is used to describe the dislocation nucleation:

$$P = \sum_{i=1,6} |\mathbf{R}_i + \mathbf{R}_{i+6}|^2, \tag{5}$$

where $\mathbf{R}_i$ and $\mathbf{R}_{i+6}$ are the vectors or bonds corresponding to the six pairs of opposite nearest neighbors in the fcc lattice. The 12 nearest-neighbor vectors for each atom are first determined in an undistorted bulk fcc lattice with the orientation of the slab. The analogous set of 12 vectors for each atom in the distorted lattice $\mathbf{R}_i$ is then generated by finding those neighbors in the distorted lattice with vectors closest in distance to the undistorted nearest-neighbor vectors. It is possible that this set will contain duplicates or non-nearest neighbors if a given atom has fewer than 12 nearest neighbors or a very distorted local environment. Each of the equal and opposite pairs of vectors is added together; then the sum of the squares of the six resulting vectors is calculated. This final number, which is a measure of the departure from centrosymmetry in

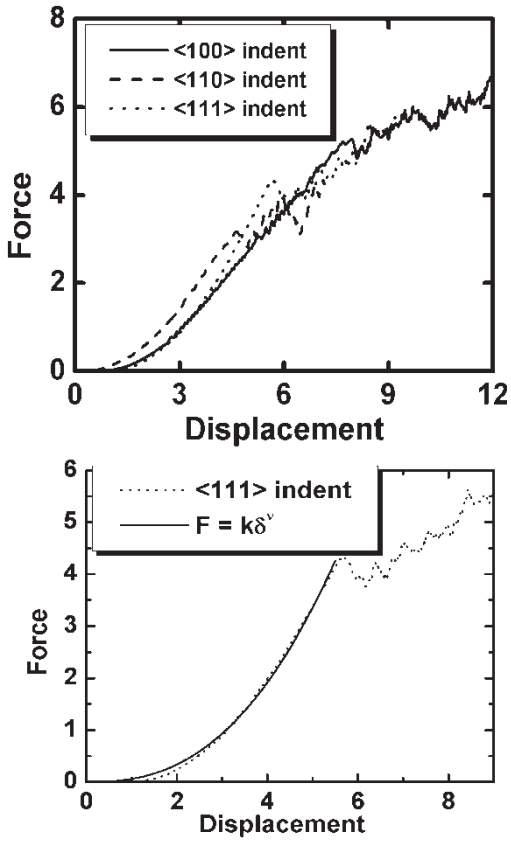

Figure 4. Top panel: indentation force vs. displacement curves in the three orientation directions. The indenter velocity is approximately 67 m/s and its diameter is 5.0 nm. Bottom panel: general power law curve fit to the elastic deformation in the ⟨111⟩ indentation, where $k = 0.06$ and $\nu = 2.5$. At the low velocity, the higher order power law curve fits the elastic deformation better than the Hertzian curve. See figure 2 caption for units.

the immediate vicinity of any given atom, is used to determine if it is near a defect [9].

The centrosymmetry parameter, P, is useful to distinguish partial dislocations and stacking faults [9]. The range of values from 0.5 to 4.0 represents partial dislocations and the range between 4.0 and the values of the surface atoms is defined as stacking faults [9]. In a perfect nickel crystal lattice, P is zero for all atoms. It is 24.78 Å^2 for the surface atoms in the ⟨100⟩ orientation, 30.88 Å^2 and 6.11 Å^2 for the surface atoms in the ⟨110⟩ orientation, and 18.59 Å^2 for the surface atoms in the ⟨111⟩ orientation. The ⟨110⟩ orientation has two P-values because the two layers of atoms have different numbers of neighbors. These values assume that the distance to the nearest neighbor does not change in the vicinity of the defects.

Figure 5 shows early dislocation nucleations in the three crystal orientations. For the ⟨100⟩ orientation, dislocation nucleation started with stacking faults in the (111) plane. This slip plane agreed with that of the shocked fcc single crystal deformation [1]. Table 2 shows the centrosymmetry values for all the atoms in figure 5. These results suggest that the dislocations propagate non-symmetrically, evolving into mixed modes with stacking faults and partial dislocations. For the ⟨110⟩ orientation, dislocation nucleation started early at the smallest displacement and propagated as partial dislocations. This slip direction agreed with that of the shocked fcc single crystal deformation [1]. For the ⟨111⟩ orientation, the initiation of dislocation nucleation took the longest time among the three orientations, propagating as mixed modes of partial dislocations and stacking faults. The centrosymmetry parameter was useful in discriminating the modes of deformation but did not provide helpful information on the Burgers vectors of dislocations. The slip vector defined by Zimmerman *et al.* [16] is known to be useful for calculating the Burgers vectors of dislocations. A slip vector model is now under investigation to calculate the Burgers vectors.

4. Conclusions

Using molecular dynamics simulations with a system size of about 400,000 atoms, I studied the anisotropic features of nanoindentation of nickel single crystals at the surfaces in the three crystallographic orientations:⟨100⟩, ⟨110⟩, and ⟨111⟩. Atomic interactions of the system were described using Voter's tabular form of the EAM potential. The indenter tip interacting with the system surface was described using the strong repulsive potential model to simulate the effect of a passivation layer. Anisotropic parameters at the surfaces were investigated as a function of indenter size and velocity in the three crystal orientations.

The force–displacement curves followed the power law solutions for elastic deformation in general. At the indenter velocity of approximately 670 m/s, the Hertzian power law solution, $F = k\delta^{1.5}$, described the elastic deformation for all three orientations. However, at the low velocity of approximately 67 m/s, the higher power law solution, $F = k\delta^{2.5}$, provided a better fit for the elastic curves. Thus, elastic behavior was dependent on the indenter velocity. The orientation dependency of the hardness was analyzed quantitatively by calculating the micro modulus, k. The discrete yield phenomena were different for the three different orientations. Thus, the results showed the dependency of anisotropic elastic–plastic deformation on the indenter size, velocity, and crystal orientation.

The centrosymmetry parameter was used to quantitatively discriminate the modes of deformation. For the ⟨100⟩ orientation, dislocation nucleation started as stacking faults in the two (111) surfaces. However, the dislocation propagation occurred non-symmetrically and soon evolved into mixed modes of stacking faults and partial dislocations. For the ⟨110⟩ orientation, dislocation nucleation occurred as partial dislocations. For the ⟨111⟩ orientation, dislocation nucleation took the longest time among the three orientations, starting as partial dislocations. However, the deformation pattern was different from that of the ⟨110⟩ orientation: the two dislocation

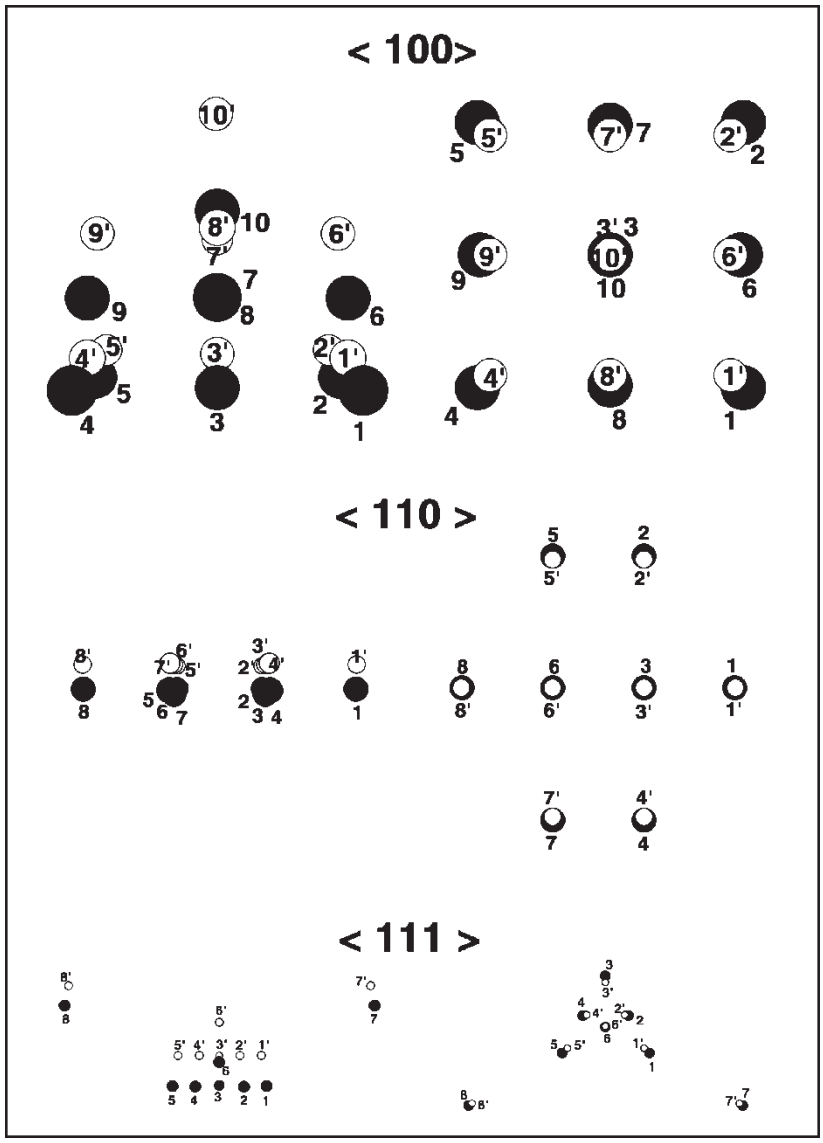

Figure 5. Dislocation nucleations at the times of 28.5, 20.0, 46.0, and at the force of 2.604, 2.363, and 6.734 from figure 3 for the three crystal orientations, ⟨100⟩, ⟨110⟩ and ⟨111⟩ from top to bottom, respectively. White circles are undistorted atoms and black circles are the corresponding distorted atoms. The indenter is moving with a constant velocity from top to bottom in the vertical direction (z-axis). The left-hand column shows the active view similar to the plane normal view to the x-axis, and the right-hand column is the top view. 10, 8, and 8 atoms are involved in the deformation for the ⟨100⟩, ⟨110⟩ and ⟨111⟩ orientations, respectively. Atoms with $P > 0.5$ are selected. The atomic number and its P-value are shown in table 2. The primed number is the corresponding undistorted atom number. The atom size in the picture is proportional to the deformed area in the crystal. The centrosymmetry parameter is useful for discriminating different deformation modes, but it fails to provide information on the Burgers vectors, which are not clearly shown in the picture.

modes, partial dislocation and stacking faults, occurred immediately and almost simultaneously. The results for the slip plane and slip direction agreed with those observed in the shocked nickel single crystals.

Table 2. The centrosymmetry, P-values at the dislocation nucleation in three crystal orientations. The atom number corresponds to that in figure 5.

Atom #	1	2	3	4	5	6	7	8	9	10
⟨100⟩	4.81	4.81	5.32	4.81	4.81	4.75	4.75	4.75	5.75	14.00
⟨110⟩	0.82	0.63	0.67	0.63	0.63	0.67	0.63	0.82		
⟨111⟩	0.57	0.55	0.95	0.55	0.57	0.72	0.51	0.51		

Acknowledgements

Art Voter is thanked for the kindness of giving his package of EAM potential models for fcc metals and their alloys. Steve Stuart is thanked for his helpful conversations and support.

References

[1] Oyeon Kum. Orientation effects in shocked nickel single crystals via molecular dynamics. *J. Appl. Phys.*, **93**, 3239 (2003).
[2] Oyeon Kum. Calculation of shock waves and temperatures of fcc single crystals (nickel) using large-scale molecular dynamics.

Proceedings of the 2003 Nanotechnology Conference and Trade Show, **2**, 538 (2003).
[3] L. Nanis, "Method of coating smooth electroless nickel on magnetic memory disks and related memory devices", US Patent application: 20020061424, Kind code: A1, US patent and trade-mark office 38 (2002)
[4] S.G. Corcoran, R.J. Colton, E.T. Lilleodden, W.W. Gerberich. Anomalous plastic deformation at surfaces: nanoindentation of gold single crystals. *Phys. Rev. B*, **55**, R16057 (1997).
[5] A. Gouldstone, H.J. Koh, K.Y. Zeng, A.E. Giannakopoulous, S. Suresh. Discrete and continuous deformation during nanoindentation of thin films. *Acta. mater.*, **42**, 2277 (2000).
[6] J. Belak, D.B. Boercker, I.F. Stowers. Simulation of nanometer-scale deformation of metallic and ceramic surfaces. *MRS Bull.*, **18**, 55 (1993).
[7] D.W. Brenner, S.B. Sinnott, J.A. Harrison, O.A. Shenderova. Simulated engineering of nanostructures. *Nanotechnology*, **7**, 161 (1996).
[8] R. Pérez, M.C. Payne, A.D. Simpson. First principles simulations of silicon nanoindentation. *Phys. Rev. Lett.*, **75**, 4748 (1995).
[9] C.L. Kelchner, S.J. Plimpton, J.C. Hamilton. Dislocation nucleation and defect structure during surface indentation. *Phys. Rev. B*, **58**, 11085 (1998).
[10] A.F. Voter, Los Alamos Unclassified Technical Report, #LA-UR93-3901 (1993).
[11] R.C. Longo, C. Rey, L.J. Gallego. Molecular dynamics study of the melting behavior of seven-atom clusters of fcc transition and noble metals on the (111) surface of the same metal using the embedded atom model. *Surface Sci.*, **459**, L441 (2000).
[12] M.M.G. Alemany, C. Rey, L.J. Gallego. A molecular dynamics study of the thermodynamic properties of liquid Ni using the Voter and Chen version of the embedded atom model. *J. Chem. Phys.*, **109**, 3568 (1998).
[13] S.J. Zhou, P.S. Lomdahl, A.F. Voter, B.L. Holian. Three-dimensional fracture via large-scale molecular dynamics. *Eng. Frac. Mech.*, **61**, 173 (1998).
[14] C.L. Liu, J.M. Cohen, J.B. Adams, A.F. Voter. EAM study of surface self-diffusion of single adatoms of fcc metals, Ni, Cu, Al, Ag, Au, Pd, and Pt. *Surface Sci.*, **253**, 334 (1991).
[15] P. Tangyunyong, R.C. Thomas, J.E. Houston, T.A. Michalske, R.M. Crooks, A.J. Howard. Nanometer-scale mechanics of gold-films. *Phys. Rev. Lett.*, **71**, 3319 (1993).
[16] J.A. Zimmerman, C.L. Kelchner, P.A. Klein, J.C. Hamilton, S.M. Foiles. Surface step effects on nanoindentation. *Phys. Rev. Lett.*, **87**, 165507-1–165507-4 (2001).